Research Square

Preprints are preliminary reports that have not undergone peer review.
They should not be considered conclusive, used to inform clinical practice,
or referenced by the media as validated information.

Finite-Time Barrier Function-Based Sliding Mode Control for Trajectory Tracking of Autonomous Sailboat

Mohammad Reza Jalili
Malek Ashtar University of Technology
Ahmad Reza Vali
Malek Ashtar University of Technology
Mohammad Ali Alirezapouri
Malek Ashtar University of Technology
Hossein Nourmohammadi
hnourmohammadi@mut.ac.ir
Malek Ashtar University of Technology

Research Article

Keywords: Autonomous Sailboat, Finite-Time Sliding Mode Control, Fast Reaching Law, Barrier Function, Lyapunov Stability

Posted Date: July 20th, 2026

DOI: https://doi.org/10.21203/rs.3.rs-10295799/v1

License: This work is licensed under a Creative Commons Attribution 4.0 International License.
Read Full License

Additional Declarations: No competing interests reported.

Finite-Time Barrier Function-Based Sliding Mode Control for Trajectory Tracking of Autonomous Sailboat

Mohammad Reza Jalili[1] , Ahmad Reza Vali[1], Mohammad Ali Alirezapouri[1], Hossein Nourmohammadi[*2]

Abstract

Autonomous sailboat navigation poses significant challenges due to its inherent nonlinear dynamics, underactuated characteristics, as well as its high sensitivity to unknown environmental disturbances. To address these issues, this paper proposes a novel finite-time barrier function (FTBF)-based sliding mode control (SMC) strategy tailored for simultaneous heading and speed control of a class of autonomous sailboat. Specifically, by integrating a novel fast-reaching law with finite-time terminal sliding mode control, the proposed method utilizes analytical proofs to guarantee accelerated system convergence to the sliding manifold. Furthermore, a barrier function is embedded within the SMC framework to explicitly constrain system states within predefined bounds, thereby ensuring operational safety during transient phases. Rigorous stability analysis, grounded in Lyapunov stability theory, establishes the finite-time convergence of the closed-loop errors to the equilibrium point. Comprehensive simulation results demonstrate that the proposed controller significantly outperforms conventional asymptotic methods in terms of convergence speed, disturbance rejection capabilities, and path-tracking accuracy.

Keywords: Autonomous Sailboat, Finite-Time Sliding Mode Control, Fast Reaching Law, Barrier Function, Lyapunov Stability.

* Corresponding Author (H. Nourmohammadi)

E-mail addresses: mohammadreza2833@gmail.com (M.A. Jalili), ar.vali@mut.ac.ir (A.R. Vali), maa_pouri@mut.ac.ir (M.A. Alirezapouri), hnourmohammadi@mut.ac.ir (H. Nourmohammadi).

[1] *Malek Ashtar University of Technology, Department of Electrical Engineering, Tehran, Iran*

[2] *Malek Ashtar University of Technology, Northern research Center for Science & Technology, Fereydunkenar, Iran*

Abbreviations

6-DOF	Six Degrees of Freedom
AUV	Autonomous Underwater Vehicle
CBF	Control Barrier Function
COE	Center of Effort
DP	Dynamic Positioning
ERL	Extended Reaching Law
ERLSMC	Extended Reaching Law Sliding Mode Control
FTBF	Finite-Time Barrier Function
FTSMC	Finite-Time Sliding Mode Control
MSV	Marine Surface Vehicle
ODE	Ordinary Differential Equation
RMS	Root Mean Square
SMC	Sliding Mode Control
TSMC	Terminal Sliding Mode Control
UMV	Unmanned Marine Vehicle

1 Introduction

Autonomous sailboats have emerged as pivotal assets for long-duration marine missions, ranging from oceanographic monitoring and environmental surveillance to distinct search-and-rescue operations. Unlike motor-propelled vessels, their capacity to harness wind propulsion renders them uniquely suitable for energy-efficient, extended deployments. However, this dependence on aerodynamic forces introduces significant stochasticity, as unpredictable wind and wave conditions impose complex nonlinear dynamics and strict underactuated constraints on the control system design (Sun et al., 2025). Addressing these challenges necessitates the development of advanced robust control methodologies capable of maintaining system performance and stability in the presence of model uncertainties, external disturbances, and actuator constraints (Tipsuwan et al., 2023).

Sliding Mode Control (SMC) is a nonlinear robust technique that utilizes a discontinuous control law to drive the system's states toward a predefined sliding surface and maintain them on it, thereby ensuring convergence to the desired equilibrium (Sabet and Nourmohammadi, 2026). This method has attracted considerable attention in recent years owing to its straightforward design and strong robustness against both model uncertainties and external disturbances. However, conventional SMC is limited by its asymptotic convergence property, meaning the system only reaches the desired state as time approaches infinity (Moulay et al., 2022). To overcome this limitation, the concept of finite-time control has been developed, which guarantees that the system achieves its control objectives within a specified and bounded time interval. This approach has been successfully integrated into the sliding mode control framework, leading to the development of Finite-Time Sliding Mode Control (FTSMC) (Huang et al., 2024). While FTSMC enhances convergence speed and maintains robustness, in many existing designs the actual settling time can still be relatively long. Therefore, there remains a need to develop improved sliding mode strategies that guarantee faster convergence in finite time while preserving robustness and simplicity in implementation.

Barrier function-based control is a modern technique in control systems designed to ensure safety by enforcing constraints on a system's behavior (Ames et al., 2016). Barrier functions are mathematical constructs that act as virtual boundaries. These functions approach infinity as the system state gets close to unsafe regions, effectively preventing the system from crossing into them (Ovalle et al., 2025). By integrating these functions into the control design, engineers can simultaneously maintain safety-critical constraints and achieve desired performance goals. This is the main reason for highly appealing real-time applications of the barrier function-based control in autonomous vehicles. The key strength of this approach lies in its safety ability. However, a significant challenge is designing or selecting barrier functions that accurately define the system's safety boundaries and align well with its dynamics (Shao et al., 2022).

There are numerous researches in the literature that have been devoted to using SMC for marine systems. Some studies have been conducted to investigate its usefulness in terms of trajectory tracking accuracy and robustness. Chen et al. proposed a robust control strategy for the positioning of marine vessels in the presence of uncertainties and input nonlinearities (Chen et al., 2013). A sliding mode control approach is utilized to maintain system performance in the presence of actuator degradation. The proposed controller is specifically designed to compensate for the reduced thrust caused by faulty thrusters, ensuring robust trajectory tracking under fault conditions. In (Yan et al., 2021), a trajectory tracking control strategy was developed for autonomous surface vehicles facing unknown boundary model uncertainties. Neural networks were employed to approximate these uncertainties, and a barrier function-based sliding mode control was designed to ensure robust tracking performance. Wang et al. proposed a path-following control method for autonomous underwater vehicles subject to unknown input nonlinearities (Wang et al., 2023). A command-filtered back-stepping approach was developed, incorporating actuator nonlinearity compensation. Additionally, barrier functions have been used to ensure that the system meets prescribed performance requirements. Adaptive neural network-based optimized control has been addressed in (Shi et al., 2024)

for dynamic positioning (DP) of marine vessels operating under ocean disturbances. The neural network was applied to estimate unknown system dynamics. Additionally, barrier functions are incorporated to ensure the safety and constraint satisfaction of the closed-loop system.

Several studies can be addressed in the literature that have been devoted to control challenges in autonomous sailboats. Abrougui et al. proposed a feedback linearization-based algorithm for the heading and sail angle control of an autonomous sailboat (Abrougui et al., 2019b). A main strength of this research is its thorough modeling and clear explanation of the sailboat's dynamic behavior, which provides a solid foundation for controller design. In another work, combining sliding mode control with feedback linearization, an applied autopilot algorithm has been developed for an autonomous catamaran sailboat (Abrougui et al., 2019a). Although this study does not consider system uncertainties and external disturbances, it represents one of the first attempts to apply SMC to this type of vessel.

Some research works have focused on finite-time control techniques in marine systems because of their capability to ensure fast convergence and improved robustness compared to conventional control methods. In (Zhu et al., 2020), the finite-time tracking control problem of underactuated marine surface vehicles with input saturation has been studied. The input saturation nonlinearity was approximated using the Gaussian error function. By employing an adaptive vector-backstepping controller, a novel adaptive finite-time tracking control law was designed to ensure fast and robust tracking performance despite input constraints. By combining finite-time control, event-triggered control, and backstepping design methods, a novel fault-tolerant control scheme has been developed in (Meng et al., 2024) for underactuated MSVs. The research in (Huang et al., 2024) focused on resilient sliding mode method to achieve finite-time control of an unmanned marine vehicle (UMV). A Takagi–Sugeno fuzzy model was developed to represent the nonlinear dynamics of the UMV, while the stochastic actuator failure was characterized by a continuous Markov process.

Despite the extensive application of Sliding Mode Control (SMC) in marine robotics, conventional SMC frameworks typically guarantee only asymptotic convergence, implying that system states reach the equilibrium theoretically as time approaches infinity. While Finite-Time SMC (FTSMC) addresses this limitation, existing FTSMC designs often fail to explicitly enforce safety constraints during the reaching phase. This presents a critical safety risk in real-world scenarios where overshoot or state violations can lead to capsizing or collision. Consequently, a significant gap remains in the literature regarding control frameworks that simultaneously ensure rapid finite-time convergence and rigorous state constraints via barrier functions, particularly for the highly nonlinear dynamics of autonomous sailboats.

To bridge this gap, this paper proposes a robust Finite-Time Barrier Function-Based SMC scheme. The main contributions of this work can be summarized as follows:

- A novel fast-reaching law is developed based on finite-time terminal sliding mode concepts, which analytically guarantees strictly bounded convergence time, superior to conventional exponential reaching laws.
- A barrier function is seamlessly integrated into the control design to enforce hard states constraints, thereby ensuring operational safety without requiring simplistic assumptions about disturbance bounds.
- Rigorous stability analysis is performed using Lyapunov theory to prove the finite-time stability of the closed-loop system under model uncertainties.

2 Sailboat mathematical model

In this section, the mathematical model, underlying assumptions, and control objectives for the robust sailboat's control are presented. The sailboat is a six-degree-of-freedom (6-DOF) system, but this system can be described by 4DOF dynamic model with logical and physical assumptions. Fig. 1 shows an overall view of the sailboat with its main parts such as body, sail, and rudder. The reference frames used for kinematic and dynamic modeling of this system are navigation frame (n-frame) and body-frame (b-frame) that represented in Fig.1 (Nourmohammadi and Sabet, 2025). The kinematic and dynamic parameters governing the sailboat's behavior are detailed in Table 1. These parameters encompass hydrodynamic coefficients, inertial properties, and geometric dimensions essential for the 4-DOF model.

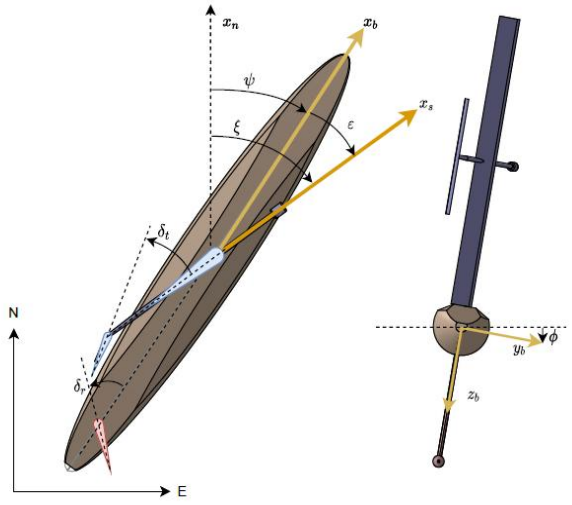


Fig. 1. Overall view of the sailboat with the main Reference coordinates frames (Jalili et al., 2024).

Table 1 Sailboat's dynamic model notation

Notation	Description
V_w, γ	Wind speed and direction
G	Boat's center of gravity
CoE	Center of effort of the sail
(x_s, y_s, z_s)	Sail's COE position in (b-frame)
(x_r, y_r, z_r)	Rudder's COE position in (b-frame)
(x, y)	Sailboat's center of gravity coordinates
(ψ, φ)	Heading and roll angle in the (n-frame)
δ_s	Sail opening angle in (b-frame)
δ_r	Rudder angle in (b-frame)
u, v	Surge and sway motion in (b-frame)
r, p	Yaw and roll rate in (b-frame)
f_s	Aerodynamic force of the wind applied on the sail in the (b-frame)
f_r	Hydrodynamic force of the water applied on the rudder in the (b-frame)
d_1, d_2	External disturbance on sail and rudder
p_1, p_2	Water friction in (b-frame)
p_4	Lift coefficient of the sail
p_5	Lift coefficient of the rudder
p_6	Distance between the mast and the COE
p_7	Distance between the boat's center of gravity and the mast
p_8	Distance between G and the rudder
p_9	Mass of the boat
p_{10}	Moment of inertia around Z-axis
p_{11}	Moment of inertia around X-axis
p_{12}	Roll friction coefficient
p_{13}	Length of the equivalent pendulum in roll motion
$X_{\dot{u}}, Y_{\dot{v}}, N_{\dot{r}}, K_{\dot{p}}$	Added mass in (b-frame)

Under the aforementioned simplifying assumptions, the state-space representation of the sailboat's 4-DOF dynamics encompassing surge, sway, roll, and yaw motions can be expressed as follows (Jaulin and Bars, 2013):

1) The boat is modeled as a rigid body with four degrees of freedom including surge, sway, roll, and yaw.
2) Environmental effects such as waves and ocean currents are neglected in the model.
3) Added mass coefficients are considered as constant.
4) Both the sail and rudder are assumed to be rigid foils.
5) Frictional forces are represented using linear damping terms in the dynamic equations of the sailboat.
6) The water flow near the rudder is assumed to be aligned with the boat's heading direction.

$$
\begin{aligned}
\dot{x} &= u\cos\psi - v\sin\psi\cos\varphi \\
\dot{y} &= u\sin\psi - v\cos\psi\cos\varphi \\
\dot{\psi} &= r\cos\varphi \\
\dot{\varphi} &= p \\
\dot{u} &= \frac{f_s\sin\delta_s - f_r\sin\delta_r - c_1 u}{c_9 - X_{\dot{u}}} \\
\dot{v} &= \frac{-f_s\cos\delta_s + f_r\sin\delta_r - c_2 v}{c_9 - Y_{\dot{v}}} \\
\dot{r} &= \frac{(c_6 - c_7\cos\delta_s)f_s - p_8 f_r\cos\delta_r + p_3 r}{c_{10} - N_{\dot{r}}} \\
\dot{p} &= \frac{z_s f_s\cos\delta_s\cos\phi - c_{13}c_9 g\sin\phi + c_{12}p}{c_{11} - K_{\dot{p}}} \\
\dot{\delta}_s &= u_1 + d_1 \\
\dot{\delta}_r &= u_2 + d_2
\end{aligned}
\tag{1}
$$

where,

$$
\begin{aligned}
f_s &= p_4(V_w\sin(\psi - \gamma + \delta_s) - u\sin\delta_s) \\
f_r &= p_5 u^2\sin\delta_r
\end{aligned}
\tag{2}
$$

Let the state vector be defined as $\mathbf{X} = [x \quad y \quad \psi \quad \varphi \quad u \quad v \quad r \quad p]^T$, where (x, y) denotes the inertial position, and (ψ, φ) represents the heading and roll angles, respectively. The control input vector $\mathbf{U} = \begin{bmatrix} \delta_s \\ \delta_r \end{bmatrix}$ consists of the sail and rudder angles, which serve as the primary actuators.

In the dynamic model of presented in Eq.1, all nonlinear functions satisfy the Lipschitz continuity condition, which implies that meaning there exists a constant $L_f > 0$ such that $|f(x) - f(y)| \le L_f |x - y|$. An appropriate controller should be developed for both the heading and the sail's opening angle.

3 Control of autonomous sailboats

In this section, first, a terminal sliding surface is designed to ensure finite-time convergence of tracking errors. Then, a novel fast reaching law is introduced, specifically proposed to enhance the convergence speed while maintaining robustness against external disturbances. In addition, a barrier function-based sliding mode control approach is developed to handle state constraints effectively while preserving the robustness property. This method ensures that the system states remain within predefined safe bounds during operation. Stability analysis of the proposed controller is carried out using Lyapunov direct method (Zhang et al., 2025). In Fig. 2, the structure of the control system of the sailboat is illustrated.

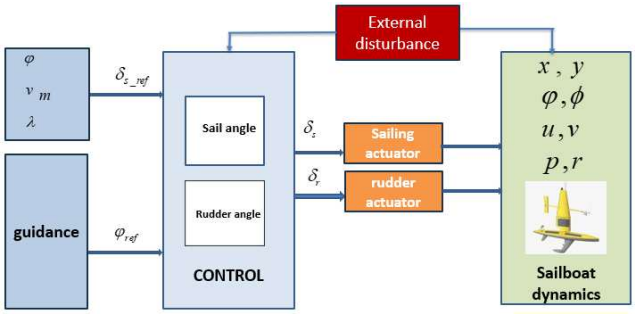


Fig. 2. Sailboat control system block diagram

The controller ensures convergence to the desired sail opening angle, $\delta_{s\,\mathrm{Ref}}$, and heading, ψ_{Ref}, thereby steers the sailboat to its intended destination. Accordingly, the following errors are defined:

$$\begin{aligned} e_1 &= \delta_s - \delta_{s\,\mathrm{Ref}} \\ e_2 &= \psi - \psi_{\mathrm{Ref}} \end{aligned} \tag{3}$$

To facilitate controller design, the error signals e_1 and e_2 are successively differentiated with respect to time until the control input explicitly appears in the resulting expressions. So,

$$\dot{e}_1 = \dot{\delta}_s - \dot{\delta}_{s\,\mathrm{Ref}} = u_1 + d_1 - \dot{\delta}_{s\,\mathrm{Ref}} \tag{4}$$

It is observed that a single time differentiation of the error signal e_1 is sufficient, as the control input u_1 appears explicitly in the first derivative. This indicates that the relative degree of the system with respect to e_1 is one, allowing for direct control input design at this level. However, the control input does not appear in the first derivative of e_2. The error e_2 must be differentiated three times so that the control input explicitly emerges, indicating a relative degree of three. So,

$$\ddot{e}_2 = f(\mathbf{X}) + g(\mathbf{X})u_2 + D(\mathbf{X},t) - \ddot{\psi}_{\mathrm{Ref}} \tag{5}$$

where,

$$\begin{aligned} f(\mathbf{X}) &= -2\left(\frac{(p_6 - p_7\cos\delta_s)f_s - p_8 f_r \cos\delta_r + p_3 r}{p_{10} - N_{\dot{r}}}\right) p\sin\varphi \\ &\quad - r\cos\varphi\, p^2 - r\sin\varphi\,\dot{p} \\ &\quad + \frac{p_7\sin\delta_s\dot{\delta}_s f_s + (p_6 - p_7\cos\delta_s)\dot{f}_s - p_8\dot{f}_r\cos\delta_r + p_3\dot{r}}{p_{10} - N_{\dot{r}}} \\ g(X) &= \frac{p_8 f_r \sin\delta_r}{p_{10} - N_{\dot{r}}} \\ D(X,t) &= \frac{p_8 f_r \sin\delta_r}{p_{10} - N_{\dot{r}}} d_2(t) \end{aligned} \tag{6}$$

Owing to the common presence of environmental disturbances that perturb the control effort, the external disturbances, (d_1, d_2), are incorporated as additive terms alongside the control inputs, (u_1, u_2). It is assumed that the external disturbances, (d_1, d_2) and consequently (d_1, D_2), and their first-time derivatives, are bounded as follows:

$$\begin{aligned} |d_1|_\infty &\le \omega_1 \\ |D_2|_\infty &\le \omega_2 \\ |\dot{d}_1|_\infty &\le \omega_3 \\ |\dot{D}_2|_\infty &\le \omega_4 \end{aligned} \tag{7}$$

where, $(\omega_1, \omega_2, \omega_3, \omega_4)$ are positive constants and $|...|_\infty$ denotes the infinity norm. The reference signals, $\delta_{s\,\mathrm{Ref}}$ and ψ_{Ref}, and their time derivatives are considered bounded for all time of $t \ge 0$.

Furthermore, the required conditions that guarantee the global finite-time stability of the equilibrium point in the dynamic system, $\dot{\boldsymbol{x}} = f(\boldsymbol{x}(t))$, The sufficient conditions guaranteeing global finite-time stability are formalized in the following Lemma.

Lemma 1: Consider the nonlinear system $\dot{\mathbf{x}} = \boldsymbol{f}(\mathbf{x}(t))$. If there exists a continuous, positive-definite Lyapunov function $\mathbf{V}(\mathbf{x})$ satisfying the differential inequality, where there are positive constants $c > 0$ and $\alpha \in (0,1)$ for which:

$$\dot{\mathbf{V}}(\mathbf{x}) \le -c(\mathbf{V}(\mathbf{x}))^\alpha, \quad \forall \mathbf{x} \in \mathbb{R}^n \tag{8}$$

Under these conditions, the origin is a globally finite-time stable equilibrium point of the system and the settling time $T(\mathbf{x}_0)$ satisfies:

$$T(\mathbf{x}_0) \le \frac{1}{c(1-\alpha)}[\mathbf{V}(\mathbf{x}_0)]^{1-\alpha} \tag{9}$$

for any initial condition of $\mathbf{x}_0$.

3.1 Proposed TSMC with enhanced reaching law

Error dynamics associated to the sail's opening angle of the above autonomous sailboat has been presented in Eq. 4. In order to design the sliding mode controller for the sail's opening angle the following sliding manifold is introduced.

$$s_1 = e_1 + c\,\mathrm{sig}^\beta\left(\int_0^t e_1 dt\right) \tag{10}$$

where, $\mathrm{sig}^\beta(x) = x^\beta \mathrm{sgn}(x)$, and $\mathrm{sgn}(x)$ is the well-known sign function. Also, c and β are real numbers satisfying $c > 0$ and $0 < \beta < 1$.

Similarly, the following sliding manifold is designed for the heading direction control of the autonomous sailboat.

$$s_2 = \ddot{e}_2 + c_1 \operatorname{sig}^{\beta_1}(\dot{e}_2) + c_2 \operatorname{sig}^{\beta_2}(e_2) \tag{11}$$

where, c_1 and c_2 are positive numbers. Also, β_1 and β_2 are real constants satisfying $0 < \beta_1, \beta_2 < 1$.

Now, consider the sailboat's dynamic model described by Eq. 1, together with the tracking errors of Eq. 5. Let the sliding surfaces, s_1 and s_2, be defined as in Eq. 10 and Eq. 11. Using the following control laws,

$$\begin{aligned} u_1(t) &= \dot{\delta}_{s\,\mathrm{Ref}} - c\, sig^{\beta-1}(\textstyle\int e_1 dt)e_1 + u_{dis1} \\ u_2(t) &= g^{-1}(\mathbf{X})(-f(\mathbf{X}) + \dddot{\psi}_{\mathrm{Ref}} - \\ & c_1 sig^{\beta_1-1}(\dot{e}_2)\ddot{e}_2 - c_2 sig^{\beta_2-1}(\dot{e}_2)\ddot{e}_2 + u_{dis2}) \end{aligned} \tag{12}$$

and adopting the newly proposed reaching law,

$$\begin{aligned} u_{dis1} &= -\left(\frac{k_1}{\lambda + (1-\lambda)\dfrac{\sigma(-\alpha s_1^p)}{\ln(e + s_1^p)}} + \omega_1\right)\operatorname{sgn}(s_1) \\ u_{dis2} &= -\left(\frac{k_2}{\lambda + (1-\lambda)\dfrac{\sigma(-\alpha s_2^p)}{\ln(e + s_2^p)}} + \omega_2\right)\operatorname{sgn}(s_2) \end{aligned} \tag{13}$$

the sliding surfaces s_1 and s_2 converge to zero in finite time. Accordingly, the proposed reaching law ensures faster convergence compared to exponential reaching law (Fallaha et al., 2011). Note that, in Eq. 13, σ is the well-known sigmoid function and e is the Napier's constant. Moreover, α, p, k_1, and k_2 are positive constants and λ satisfies $0 < \lambda < 1$. The time derivative of the sliding variable is determined as:

$$\dot{s}_1 = \dot{\delta}_s - \dot{\delta}_{s\,\mathrm{Ref}} + c\, sig^{\beta-1}(\textstyle\int e_1 dt)e_1 \tag{14}$$

Substituting $\dot{\delta}_s$ from Eq.1 yields:

$$\dot{s}_1 = u_1(t) + d_1(t) - \dot{\delta}_{s\,\mathrm{Ref}} + c\, sig^{\beta-1}(\textstyle\int e_1 dt)e_1 \tag{15}$$

Using Eq. 12, Eq. 13 and Eq. 14, Eq. 15 is rewritten as follows.

$$\dot{s}_1 = -\frac{k_1}{\lambda + (1-\lambda)\dfrac{\sigma(-\alpha s_1^p)}{\ln(e + s_1^p)}}\operatorname{sgn}(s_1) + d_1(t) \tag{16}$$

To verify the stability of the proposed sliding manifold, consider the following candidate Lyapunov function:

$$V_1 = \frac{1}{2}s_1^2 \tag{17}$$

Differentiating V_1 with respect to time and substituting the error dynamics from Eq.16 yields:

$$\begin{aligned} \dot{V_1} = \dot{s}_1 s_1 &= \left[-\left(\frac{k_1}{\lambda + (1-\lambda)\dfrac{\sigma(-\alpha s_1^p)}{\ln(e + s_1^p)}} + \omega_1\right)\operatorname{sgn}(s_1) + d_1(t)\right]s_1 \\ &= -\frac{k_1}{\lambda + (1-\lambda)\dfrac{\sigma(-\alpha s_1^p)}{\ln(e + s_1^p)}}|s_1| - \omega_1|s_1| + d_1(t)s_1 \le \\ &-\frac{k_1}{\lambda + (1-\lambda)\dfrac{\sigma(-\alpha s_1^p)}{\ln(e + s_1^p)}}|s_1| - \omega_1|s_1| + |d_1(t)||s_1| \end{aligned} \tag{18}$$

Based on the above a*ssumption*, it can be inferred that:

$$\begin{aligned} \dot{V_1} &\le -\frac{k_1}{\lambda + (1-\lambda)\dfrac{\sigma(-\alpha s_1^p)}{\ln(e + s_1^p)}}|s_1| - \omega_1|s_1| + \omega_1|s_1| \\ &\le -\frac{k_1}{\lambda + (1-\lambda)\dfrac{\sigma(-\alpha s_1^p)}{\ln(e + s_1^p)}}|s_1| \end{aligned} \tag{19}$$

As the function ($H(s_1) = \lambda + (1-\lambda)\dfrac{\sigma(\alpha s_1^p)}{\ln(e + s_1^p)}$) is always positive, $\dot{V_1}$ is negative definite and the stability is verified. From Eq. 18 and Eq. 19, it can be inferred that,

$$\begin{aligned} \dot{s}_1 = \frac{ds_1}{dt} &\le -\frac{k_1}{\lambda + (1-\lambda)\dfrac{\sigma(-\alpha s_1^p)}{\ln(e + s_1^p)}}\operatorname{sgn}(s_1) \\ dt &\le -\frac{\lambda + (1-\lambda)\dfrac{\sigma(-\alpha s_1^p)}{\ln(e + s_1^p)}ds_1}{k_1 \operatorname{sgn}(s_1)} \end{aligned} \tag{20}$$

Applying $\operatorname{sgn}(s_1) = 1$ for $s_1 > 0$ and also integrating from 0 to t_{r1} and $s_1(0)$ to 0 yields:

$$\int_0^{t_{r1}} dt \le -\int_{s_1(0)}^{0} \frac{\lambda + (1-\lambda)\dfrac{\sigma(-\alpha s_1^p)}{\ln(e + s_1^p)}}{k_1} ds_1 \tag{21}$$

And Eq. 21 can be rewritten as:

$$\int_0^{t_{r1}} dt \le \int_0^{s_1(0)} \frac{\lambda + (1-\lambda)\dfrac{\sigma(-\alpha s_1^p)}{\ln(e + s_1^p)}}{k_1} ds_1 \tag{22}$$

Similarly for $s_1 < 0$, it can be inferred that:

$$\int_0^{t_{r1}} dt \le \int_0^{-s_1(0)} \frac{\lambda + (1-\lambda)\dfrac{\sigma(-\alpha s_1^{\,p})}{\ln(e + s_1^{\,p})}}{k_1} ds_1 \tag{23}$$

Therefore, Eq. 22 and Eq. 23 can be united as:

$$t_{r1} \le \int_0^{|s_1(0)|} \frac{\lambda + (1-\lambda)\dfrac{\sigma(-\alpha s_1^{\,p})}{\ln(e + s_1^{\,p})}}{k_1} ds_1 \tag{24}$$

And Eq.24 can be simplified as:

$$\begin{aligned} t_{r1} &\le \int_0^{|s_1(0)|} \frac{\lambda_1}{k_1} ds_1 + \int_0^{|s_1(0)|} \frac{(1-\lambda_1)\dfrac{\sigma(-\alpha s_1^{\,p})}{\ln(e + s_1^{\,p})}}{k_1} ds_1 \\ &\le \int_0^{|s_1(0)|} \frac{\lambda_1}{k_1} ds_1 + \int_0^{|s_1(0)|} \frac{(1-\lambda_1)}{2k_1} ds_1 \\ &\le \frac{\lambda_1}{k_1} |s_1(0)| + \frac{(1-\lambda_1)}{2k_1} |s_1(0)| \end{aligned} \tag{25}$$

It can be analytically demonstrated that the proposed reaching law ensures a strictly shorter convergence time compared to the Extended Reaching Law (ERL) presented in (Fallaha et al., 2011). Specifically, analyzing the integral term in Eq. 26 reveals that:

$$t_{r\,\mathrm{ERL}} \le \int_0^{|s_1(0)|} \frac{\lambda_1 + (1-\lambda_1)e^{-\alpha|s_1|^p}}{k_1} ds_1 \tag{26}$$

where, $0 < \lambda_1 < 1$; α and p are positive constants. Now, subtracting Eq. 24 from Eq. 26 yields:

$$t_{r\,\mathrm{ERL}} - t_{r1} \le \int_0^{|s_1(0)|} \left(\frac{\lambda + (1-\lambda)e^{-\alpha|s_1|^p}}{k_1} - \frac{\lambda + (1-\lambda)\dfrac{\sigma(-\alpha s_1^{\,p})}{\ln(e + s_1^{\,p})}}{k_1} \right) ds_1 \tag{27}$$

Equation (27) can be simplified as follows:

$$t_{r\,\mathrm{ERL}} - t_{r1} \le \frac{(1-\lambda)}{k_1} \int_0^{|s_1(0)|} \left(e^{-\alpha|s_1|^p} - \frac{\sigma(-\alpha s_1^{\,p})}{\ln(e + s_1^{\,p})} \right) ds_1 \tag{28}$$

The sign of the integral must be analyzed. The integrand consists of two positive functions. The first term, $e^{-\alpha|s_1|^p}$, is a monotonically decreasing exponential function with respect to s_1, starting from 1 at $s_1 = 0$ and decreasing toward zero as s_1 increases. The second term $\dfrac{\sigma(-\alpha s_1^{\,p})}{\ln(e + s_1^{\,p})}$ is also a monotonically decreasing function. By defining,

$$f(s_1) = e^{-\alpha|s_1|^p} - \frac{\sigma(-\alpha s_1^{\,p})}{\ln(e + s_1^{\,p})} \tag{29}$$

It can be inferred that, $f(0) = 0.5$; however, for $s_1 > 0$, we need to show:

$$e^{-\alpha|s_1|^p} - \frac{1}{(1 + e^{\alpha s_1^{\,p}})\ln(e + s_1^{\,p})} > 0 \tag{30}$$

Accordingly, multiplying both sides of Eq. 30 by $(1 + e^{\alpha s_1^{\,p}})\ln(e + s_1^{\,p})$ yields:

$$(e^{-\alpha s_1^{\,p}} + 1)\ln(e + s_1^{\,p}) > 1 \tag{31}$$

Since $e^{-\alpha s_1^{\,p}} > 0$ and $\ln(e + s_1^{\,p}) > 1$, therefore $f(s_1)$ is always positive for $s_1 > 0$ and consequently, the integral of Eq.31 is positive. As a result, the difference between the reaching times $t_{r\,\mathrm{ERL}} - t_{r1}$ is positive. This indicates that the reaching time in reference (Fallaha et al., 2011) is larger compared to the proposed approach.

The proposed reaching law not only guarantees finite-time convergence to the sliding surface but also results in a strictly shorter reaching time compared to the classic method presented in (Fallaha et al., 2011). This improvement, which has been theoretically validated, demonstrates the enhanced efficiency of the new law in accelerating system response and enforcing robustness during the reaching phase. For the heading direction, the derivative of the sliding surface is:

$$\begin{aligned} \dot{s}_2 &= f(X) + g(X)u_2 - \ddot{\psi}_{\mathrm{Ref}} + c_1\beta_1 |\dot{e}_2|^{\beta_1 - 1}\ddot{e}_2 \\ &\quad + c_2\beta_2 |e_2|^{\beta_2 - 1}\dot{e}_2 \end{aligned} \tag{32}$$

By applying the control law of presented in Eq. 12, it can be rewritten as:

$$\dot{s}_2 = u_{dis\,2} + D(X, t) \tag{33}$$

Similar to the analysis of the reaching phase for sliding surface s_1, the proposed reaching law ensures fast finite-time stability.

Assume the system trajectories reach the sliding manifold $s_1, s_2 = 0$ in finite time under the proposed reaching law. Then, the sliding motion on each surface is

finite-time stable, ensuring that the reduced-order dynamics are converged to the origin $s_1, s_2 = 0$ in finite time.

Proof:

As the sliding surface defined in Eq. 10 reaches zero in finite time, we have:

$$e_1 = -c\,\mathrm{sig}^{\beta}\left(\int_0^t e_1 dt\right) \tag{34}$$

To perform the stability analysis, the following Lyapunov candidate function is defined.

$$V_2 = \frac{1}{\beta+1}\left(\left|\int_0^t e_1 dt\right|\right)^{\beta+1} \tag{35}$$

and its derivative is equal to:

$$\dot{V_2} = \left(\left|\int_0^t e_1 dt\right|\right)^{\beta} \mathrm{sgn}\left(\int_0^t e_1 dt\right) e_1 \tag{36}$$

Substituting Eq. 34, we have:

$$\begin{aligned}\dot{V_2} &= \left|\int_0^t e_1 dt\right|^{\beta} \mathrm{sgn}\left(\int_0^t e_1 dt\right)\left(-c\left|\int_0^t e_1 dt\right|^{\beta} \mathrm{sgn}\left(\int_0^t e_1 dt\right)\right) \\ &= -2c\left|\int_0^t e_1 dt\right|^{\beta+1}\end{aligned} \tag{37}$$

It can be inferred from Eq. 37, the function V_2 is negative definite and consequently s_1 is stable. Having established the reaching phase, it is now necessary to investigate the finite-time stability of the sliding surface. Accordingly, the following Lyapunov candidate is defined.

$$V_3 = \frac{1}{2}\left(\int_0^t e_1 dt\right)^2 \tag{38}$$

and its derivative can be computed as:

$$\begin{aligned}\dot{V_3} &= \left(\int_0^t e_1 dt\right) e_1 = \left(\int_0^t e_1 dt\right)\left[-c\left|\int_0^t e_1 dt\right|^{\beta} \mathrm{sgn}\left(\int_0^t e_1 dt\right)\right] \\ &= -c\left|\int_0^t e_1 dt\right|^{\beta+1} = -2^{-\frac{\beta+1}{2}} c\left[\frac{1}{2}\left(\int_0^t e_1 dt\right)^2\right]^{\frac{\beta+1}{2}} \\ &= -2^{-\frac{\beta+1}{2}} c V_3^{\frac{\beta+1}{2}}\end{aligned} \tag{39}$$

which is finite time stable according to *Lemma 1*, and the finite stability time is:

$$T < \frac{\left(V_3(0)\right)^{\frac{1-\beta}{2}}}{2^{-\frac{\beta+2}{2}} c(1-\beta)} \tag{40}$$

A similar stability analysis must now be carried out for the second sliding surface s_2, with particular attention to verifying its finite-time stability. As the sliding surface defined in Eq. 11 reaches zero in finite time, we have:

$$\ddot{e}_2 = -c_1 \mathrm{sig}^{\beta_1}(\dot{e}_2) - c_2 \mathrm{sig}^{\beta_2}(e_2) \tag{41}$$

To prove the stability of sliding surface $s_2 = 0$, the following Lyapunov function is considered:

$$V_4 = \frac{c_2}{\beta_2+1}\left|e_2\right|^{\beta_2+1} + \frac{1}{2}\dot{e}_2^2 \tag{42}$$

and its derivative is equal to:

$$\dot{V_4} = c_2\left|e_2\right|^{\beta_2} \mathrm{sgn}(e_2)\dot{e}_2 + \dot{e}_2\ddot{e}_2 \tag{43}$$

By substituting Eq. 41, we have:

$$\begin{aligned}\dot{V_4} &= c_2\left|e_2\right|^{\beta_2} \mathrm{sgn}(e_2)\dot{e}_2 + \dot{e}_2\left[-c_1 \mathrm{sig}^{\beta_1}(\dot{e}_2) - c_2 \mathrm{sig}^{\beta_2}(e_2)\right] \\ &= -c_1\left|\dot{e}_2\right|^{\beta_1+1}\end{aligned} \tag{44}$$

This is negative semi-definite for positive c_1 and β_1. From LaSalle's Invariance Theorem, consider the set where the derivative of the Lyapunov function is zero,

$$\dot{V_4} = -c_1\left|\dot{e}_2\right|^{\beta_1+1} = 0 \quad \Rightarrow \quad x_2 = 0 \tag{45}$$

On this set, the dynamics are evaluated.

$$\begin{cases}\dot{e}_2 = 0, \\ \ddot{e}_2 = -c_2 \mathrm{sig}^{\beta_2}(e_2)\end{cases} \tag{46}$$

For the trajectories to remain in this set (i.e., for the set to be invariant), it must also be $\ddot{e}_2 = 0$, which implies:

$$\mathrm{sig}^{\beta_2}(e_2) = 0 \quad \Rightarrow \quad e_2 = 0 \tag{47}$$

Therefore, $\dot{V} = 0$ is the largest invariant set in $(x_1, x_2) \in \mathbb{R}^2$. By LaSalle's Invariance principle, the equilibrium at the origin is globally asymptotically stable.

Having established the Lyapunov stability of the system in the previous section, we now strengthen this result by proving finite-time convergence to the equilibrium. According to the Lyapunov function of Eq. 42,

$$V_4 > \frac{1}{2}\dot{e}_2^2 \tag{48}$$

so,

$$\left|\dot{e}_2\right| < \sqrt{2V_4} \tag{49}$$

Taking both sides to the power of $\beta_1 + 1$:

$$\left|\dot{e}_2\right|^{\beta_1+1} < \left(2V_4\right)^{\frac{\beta_1+1}{2}} \tag{50}$$

Applying it to Eq. 45, yields:

$$\dot{V}_4 = -c_1 \left| \dot{e}_2 \right|^{\beta_1 + 1} < -c_1 \left(2V_4 \right)^{\frac{\beta_1 + 1}{2}} \tag{51}$$

which is finite time stable based on *Lemma 1*, and the upper bound of the stability finite time is achieved by:

$$T < \frac{V_4^{\frac{1-\beta_1}{2}}(0)}{2c_1(1-\beta_1)} \tag{52}$$

3.2 Proposed BFSMC

In order to enhance the control performance while ensuring that the system states remain within predefined safety bounds, this section introduces a barrier function-based sliding mode control strategy. By incorporating barrier functions into the control design, it becomes possible to enforce state constraints implicitly, preventing trajectories from violating critical limits.

To design the barrier function-based sliding mode controller, the discontinuous control laws are formulated in two distinct cases.

Case 1. For the condition where $|s| \geq \varepsilon$, the control law of Eq. 13 is adopted as the foundation for the proposed barrier function-based sliding mode control. In this case, the controller operates outside the boundary layer and ensures robust convergence of the sliding variable toward the surface.

Case 2. For the condition where $|s| < \varepsilon$, the following discontinuous control laws are employed:

$$\begin{aligned} u_{dis\,1} &= -f_{b1}\,\mathrm{sgn}(s_1) \\ u_{dis\,2} &= -f_{b2}\,\mathrm{sgn}(s_2) \end{aligned} \tag{53}$$

where, f_{b1} and f_{b2} are the barrier functions defined as follows:

$$\begin{aligned} f_{b1} &= \frac{|s_1|}{\varepsilon - |s_1|} \\ f_{b2} &= \frac{|s_2|}{\varepsilon - |s_2|} \end{aligned} \tag{54}$$

where, $\varepsilon > 0$ is a small constant that defines the thickness of the boundary layer around the sliding surface. These barrier functions grow rapidly as $|s_1|$ and $|s_2|$ approach ε, thereby preventing the sliding variable from violating the predefined boundary and ensuring that system trajectories remain within the safe region.

Finally, by combining Eq. 53 and Eq. 54 with Eq. 12, the overall formulation of the proposed barrier function sliding mode controller is advanced.

The primary advantage of the barrier function is that it eliminates the necessity for an upper bound on disturbances. Owing to the inherent properties of the barrier function, disturbances can be effectively managed without overestimation. Specifically, when the sliding variable s nears the boundary $(-\varepsilon.\varepsilon)$, the control law generates a large input to pull it back. Conversely, as $s$approaches zero, the barrier function f_b tends to zero. However, a potential drawback of the barrier function-based approach is that it may lead to large control inputs, which could result in input saturation.

Under above *Assumption* and based on the control strategy defined in Eq. 12, Eq. 13, Eq. 53 and Eq. 54, the proposed barrier function-based sliding mode controller, ensures that the sliding variables s_1 and s_2 converges to the origin while remaining within the safe region of $|s_1|, |s_2| < \varepsilon$.

Proof:

Case 1. For control inputs Eq. 12 and Eq. 13, when $|s_1| \geq \varepsilon$, we aim to demonstrate that if $|s_1(0)| \geq \varepsilon$, the sliding variable s_1 will asymptotically converge to the region of $(-\varepsilon, \varepsilon)$.

Considering the Lyapunov function of Eq. 17 and analyzing the stability under the control inputs Eq. 12, it can be proved that when $|s_1(0)| \geq \varepsilon$, the sliding variable s_1 will asymptotically converge to the boundaries in finite time.

Case 2. Where the sliding variable satisfies $|s_1| < \varepsilon$, the system operates within the boundary layer defined by the barrier function. To analyze the behavior in this region, we consider the discontinuous control law of Eq. 53 and examine the stability of s_1 to the origin using a Lyapunov-based approach.

The following Lyapunov function is considered:

$$V_5 = \frac{1}{2}s_1^2 + \frac{1}{2}\left(f_{b1}(s) - f_{b1}(0)\right)^2 \tag{55}$$

Utilizing Eq. 12 and observing that $f_{b1}(0) = 0$, the time derivative of V_5 along the system trajectories under the barrier function-based control input Eq. 53 can be evaluated as follows:

$$\begin{aligned}\dot{V_5} &= s_1\dot{s_1} + f_{b1}(s_1)\dot{f_{b1}}(s_1)\\ &= s_1(u_{dis1} + d_1(t)) + f_{b1}(s)\dot{f_{b1}}(s_1)\\ &= s_1(u_{dis1} + d_1(t)) + \\ &\quad f_{b1}(s)\left(\frac{\varepsilon}{(\varepsilon - |s_1|)^2}\right)\mathrm{sgn}(s_1)(u_{dis1} + d_1(t))\end{aligned} \tag{56}$$

Applying discontinuous control input of presented in Eq. 45 yields:

$$\begin{aligned}\dot{V_5} &= s_1(-(f_{b1} + \omega_1)\,\mathrm{sgn}(\mathrm{s}_1) + \mathrm{d}_1(t)) + \\ &\quad f_{b1}(s)\left(\frac{\varepsilon}{(\varepsilon - |s_1|)^2}\right)\mathrm{sgn}(\mathrm{s}_1)(-(f_{b1} + \omega_1)\,\mathrm{sgn}(\mathrm{s}_1) + \mathrm{d}_1(t))\\ &= -f_{b1}|s_1| - \omega_1|s_1| + \mathrm{d}_1(t)s_1 + \\ &\quad f_{b1}(s)\left(\frac{\varepsilon}{(\varepsilon - |s_1|)^2}\right)(-f_{b1} - \omega_1 + \mathrm{d}_1(t)\,\mathrm{sgn}(\mathrm{s}_1))\end{aligned} \tag{57}$$

Moreover, it can be inferred that:

$$\begin{aligned}\dot{V_5} &\le -f_{b1}|s_1| - \omega_1|s_1| + \omega_1|s_1| + f_{b1}(s)\left(\frac{\varepsilon}{(\varepsilon - |s_1|)^2}\right)(-f_{b1})\\ &\le -f_{b1}|s_1| - f_{b1}^2(s)\left(\frac{\varepsilon}{(\varepsilon - |s_1|)^2}\right)\end{aligned} \tag{58}$$

Additionally, by introducing the following parameters:

$$\sigma_1 = \sqrt{2}f_{b1}, \qquad \sigma_2 = f_{b1}(s)\left(\frac{\sqrt{2}\varepsilon}{(\varepsilon - |s_1|)^2}\right) \tag{59}$$

The derivative of the Lyapunov function can be rewritten as follows:

$$\dot{V_5} = -\sigma_1\frac{1}{\sqrt{2}}|s_1| - \sigma_2\frac{1}{\sqrt{2}}f_{b1} \le -\min\{\sigma_1, \sigma_2\}V_5^{1/2} \tag{60}$$

which is finite time stable based on *Lemma 1*, and the upper bound of the stability finite time is achieved by:

$$T < \frac{2V_5^{1/2}(0)}{\min\{\sigma_1, \sigma_2\}} \tag{61}$$

For the error dynamics of Eq. 5, sliding surface of Eq. 11 with its associated control inputs Eq. 12 and Eq. 53, the barrier function-based sliding mode control is employed. The stability analysis follows an analogous process to that of the first system, ensuring convergence to the sliding surface and system stability. Accordingly, the stability of the second system is established using the same Lyapunov-based methodology.

4 Simulation results

In this section, simulations are conducted using MATLAB/Simulink to validate the performance of the proposed control scheme for an autonomous sailboat, even in the presence of external disturbances. Associated differential equations were solved using the ODE3 solver in MATLAB by using fixed-step third-order Runge-Kutta method with a sample time of 0.01 seconds. To conduct realistic simulations, the parameters used in the sailboat's dynamic model are selected based on typical values for an autonomous sailboat as listed in Table 2. Also, the simulation control parameters are presented in Table 3.

Table 2 Sailboat's model parameters (Abrougui et al., 2019b)

Parameter	Value	Parameter	Value
p_1	$10\ kg.s\ /\ m$	p_{11}	$12.5\ kg.m^2$
p_2	$400 kg.s\ /\ m$	p_{12}	$40\ kg.m^2\ /\ rad.s$
p_3	$125 kg.m^2\ /\ rad.s$	p_{13}	$0.2\ m$
p_4	30	$X_{\dot{u}}$	-20 kg
p_5	50	$Y_{\dot{v}}$	-200 kg
p_6	0.5 m	$N_{\dot{r}}$	$-50\ kg.m^2$
p_7	0.5 m	$K_{\dot{p}}$	$-12\ kg.m^2$
p_8	1.5 m	g	$9.8\ m\ /\ s^2$
p_9	200 kg	z_s	1 m
p_{10}	$50 kg.m^2$	$x_s = y_s$	0 m

Table 3 Sailboat's control parameters

Parameter Category	Symbol	Value	Description
Environment	V_w	10 m/s	Wind Speed
	γ	$3/2\ \pi$ rad	Wind Direction
Controller Gains	k_1	1	SMC Gain (Sail)
	k_2	3.5	SMC Gain (Heading)
	λ	0.5	Reaching Law Parameter
	β	3.5	S1 sliding manifold Parameter
	β_1	3.5	S2 sliding manifold Parameter
	β_2	3.7	S2 sliding manifold Parameter
	p	0.5	Reaching Law Parameter
Barrier Function	ε_1	0.01	Safety Bounds
	ε_2	0.01	Safety Bounds
Disturbances	d_1	$1.5\sin(2t)$	External Disturbance
	d_2	0.75 $t > 8$ sec 0 otherwise	External Disturbance

The simulations are initialized with the following state vector:

$$\mathbf{X} = \begin{bmatrix}0 & 0 & 0.75\pi & 0 & 8 & 0 & 0 & 0 & 0.44\pi & 0\end{bmatrix}^T \tag{62}$$

Also, the reference signals are (Jaulin and Le Bars, 2014):

$$\psi_{\text{Ref}} = \frac{7\pi}{6}, \quad \delta_{s\,\text{Ref}} = \pi[\frac{\psi}{2\pi} + \frac{1}{4}] + \frac{\pi}{4} - \frac{\psi}{2} \tag{63}$$

4.1 Simulation results of the TSMC method

In this subsection, the results of the sliding mode control based on the terminal sliding surfaces defined in Eq. 11 and Eq. 12, employing the conventional reaching law, $u_{dis} = -k\ \text{sgn}(s)$, are presented in Figs 3 through 6.

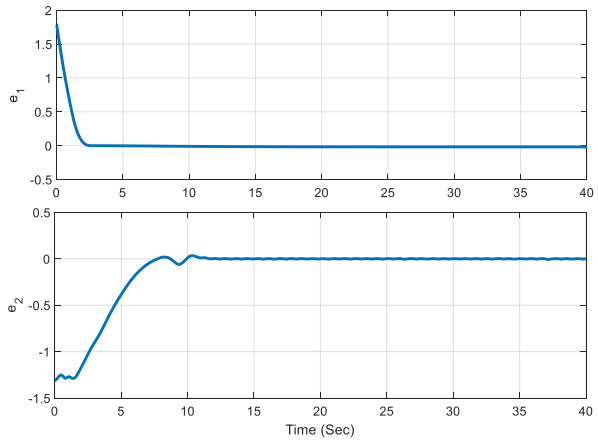


Fig. 3. Sail opening angle error, e_1, and heading angle error, e_2 under terminal sliding mode controller

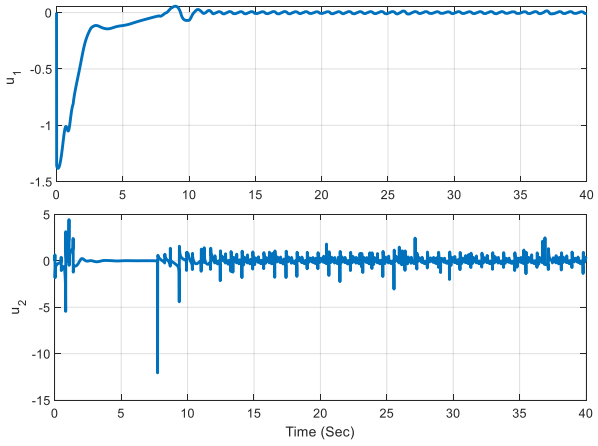


Fig. 4. Control input u_1 and u_2 generated by the terminal sliding mode controller

Fig. 3 illustrates the time evolution of the tracking errors for the sail opening angle (e_1) and heading angle (e_2). It is evident that under the proposed controller, both error signals converge asymptotically to the origin within a finite time interval. Notably, the transient response exhibits minimal overshoot and rapid settling time, corroborating the theoretical claims regarding the fast-reaching law. Furthermore, despite the injection of external disturbances at $t = 8\,s$, the control inputs depicted in Fig. 4 remain smooth and bounded. The absence of high-frequency chattering in the control signal highlights the efficacy of the barrier function in mitigating the adverse effects of discontinuous switching terms.

4.2 Simulation result of TSMC with enhanced reaching law

In this section, the results of the terminal sliding mode control employing the proposed enhanced reaching laws defined in Eq. 14 are presented and discussed.

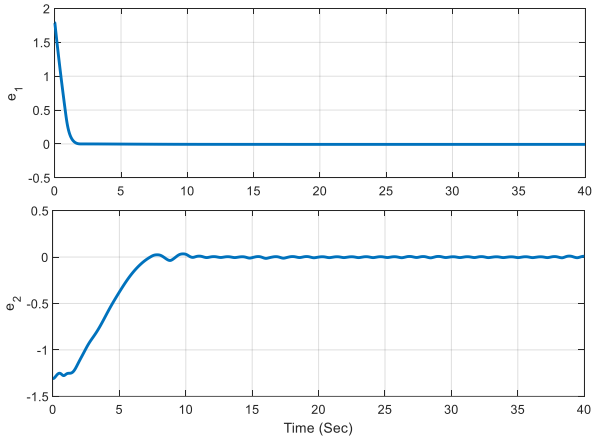


Fig. 5. Sail opening angle error, e_1, and heading error, e_2 under terminal sliding mode controller with enhanced reaching law

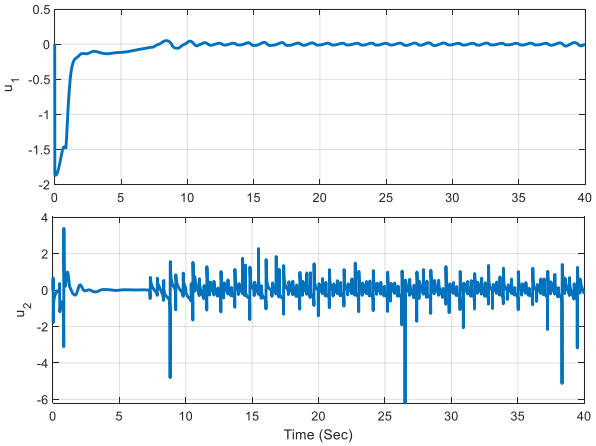


Fig. 6. Control input u_1 and u_2 generated by the terminal sliding mode controller with enhanced reaching law

As shown in Fig. 5, both the sail angle and heading angle tracking errors converge to zero with high accuracy, confirming the robustness and precision of the proposed control strategy. The transient responses exhibit rapid convergence with minimal overshoot, indicating satisfactory dynamic performance. Fig. 6 depicts the corresponding control inputs, which remain smooth and bounded throughout the entire maneuver, demonstrating the

controller's ability to suppress chattering while maintaining effective actuation.

4.3 Simulation result of BFSMC method

In this section, the results of the barrier function–based sliding mode control, designed using the control laws defined in Eq. 54, the sliding surfaces given in Eq. 11 and Eq. 12 and the enhanced reaching laws introduced in Eq. 15, are presented in Figs 7 through 11. The results are also compared with those obtained using the ERLSMC method proposed in (Fallaha et al., 2011).

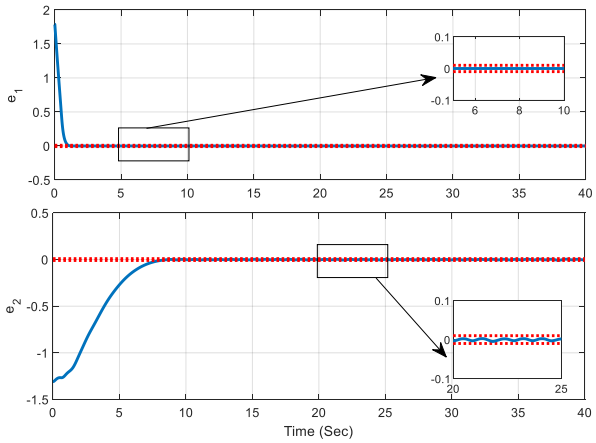


Fig. 7. Sail opening angle error, e_1 , and heading angle error, e_2

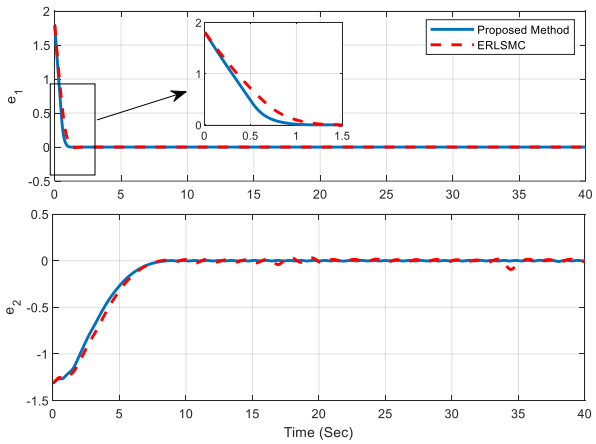


Fig. 8. Comparative results of Sail opening angle error, e_1 , and heading angle error, e_2

As illustrated in Fig. 7, the error trajectories e_1 and e_2, together with their corresponding barrier function bounds, are presented. The figure also includes zoomed-in views for both errors, showing that they consistently remain within the prescribed barrier limits throughout the operation. As shown in Fig. 8, the sail-angle tracking error e_1 converges to zero rapidly and accurately, demonstrating the controller's fast response and high precision. Similarly, the heading angle tracking error e_2 also converges to zero, albeit at a slower rate. This behavior is expected due to the more complex and nonlinear dynamics associated with heading control, as well as the greater physical difficulty in adjusting the heading angle compared with the sail angle. Nevertheless, both errors exhibit significantly faster convergence and smaller steady-state deviations compared to those obtained using the ERLSMC method (Fallaha et al., 2011), demonstrating the superior tracking capability of the proposed barrier-enhanced control scheme.

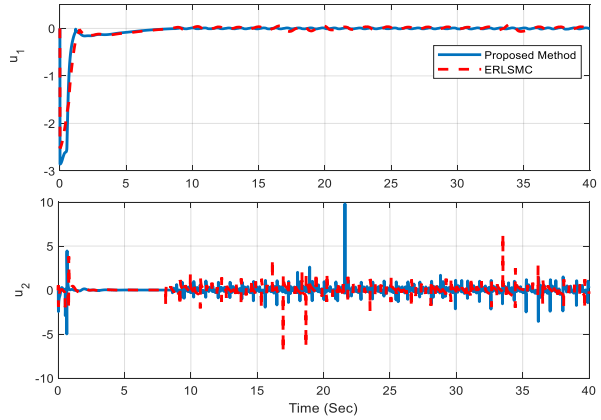


Fig. 9. Control input u_1 and u_2 generated by the barrier function-based sliding mode control

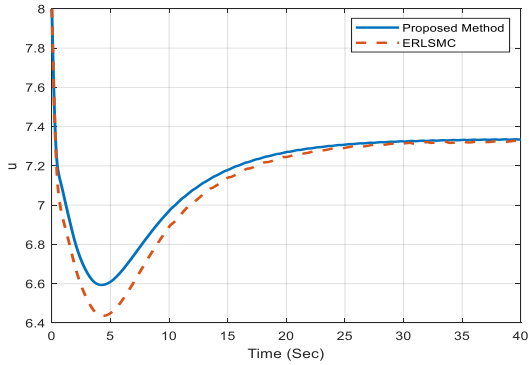


Fig.10 Comparison results of surge speed

Fig. 9 depicts the control inputs u_1 and u_2, both of which remain bounded and exhibit smooth variations without abrupt fluctuations, confirming the robustness and practicality of the proposed control law. A slight fluctuation appears in the control signals after the disturbance is applied; however, the controller effectively maintains system stability and overall performance. Importantly, the comparable magnitudes of the control efforts between the two approaches indicate that the improved tracking precision is achieved without increasing actuator demand, thus enhancing energy efficiency. Finally, Fig. 10 presents the surge speed of the sailboat, which converges to its desired value more rapidly under the proposed control

strategy than under the reference ERLSMC method (Fallaha et al., 2011), demonstrating improved responsiveness and effectiveness in regulating the vessel's forward motion.

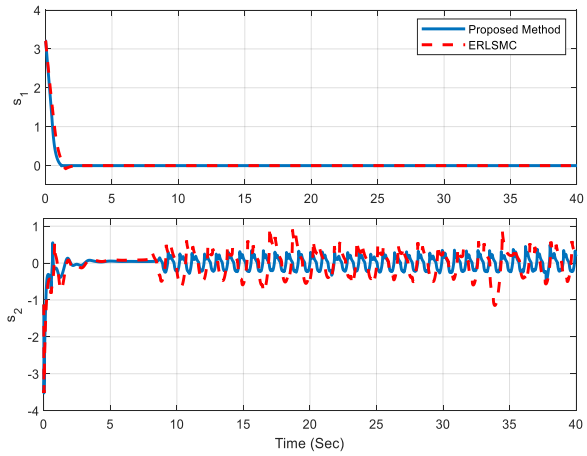


Fig. 11. Sliding surfaces s_1 and s_2

Fig. 11 illustrates the evolution of the sliding surfaces associated with both the sail and heading dynamics. The corresponding sliding variables effectively converge to zero, confirming that the system trajectories reach and remain on the designated sliding manifolds throughout the operation. A comparative analysis with the ERLSMC method proposed by (Fallaha et al., 2011) is also presented. The results clearly reveal that the proposed controller achieves faster convergence of the sliding variables and maintains the sliding condition with greater robustness, thereby ensuring improved finite-time stability and high-precision tracking performance. Finally, to quantitatively summarize these advantages, Table 4 compares key factors including rise time, RMS error, and control effort.

Table 4 Quantitative performance comparison between proposed method and ERLSMC (RMS error and settling time)

Criteria		Terminal SMC	Terminal SMC with Enhanced Reaching Law	Proposed FTBF-SMC	ERL-SMC (Fallaha et al., 2011)	Improvement (%)
Rise Time (Sec)	e_1	1.98	1.39	1.2	2	39.4
	e_2	9.11	8.88	8.7	9.5	8.4
RMS Error	e_1	0.2	0.16	0.11	0.18	38.9
	e_2	0.36	0.35	0.34	0.45	24.4
Control Effort	u_1	2.72	2.84	2.81	3.26	13.8
	u_2	9.99	9.56	9.31	9.38	0.7

Table 4 presents a comprehensive comparison among three proposed controllers including terminal SMC, terminal SMC with enhanced reaching law, and the barrier function-based SMC as well as the ERLSMC reported in (Fallaha et al., 2011). The evaluation covers rise time, root mean square (RMS) error, and control effort criteria. Overall, the proposed control schemes exhibit superior performance compared with the reference method. In terms of rise time, all proposed controllers achieve faster convergence in the tracking errors e1 e_1 and e_2 relative to ERLSMC, with the barrier function-based SMC reaching the target significantly sooner (1.2 s for e_1 and 8.7 s for e_2), indicating an enhanced dynamic response. Concerning RMS error, the proposed approaches maintain lower error magnitudes than the benchmark, reflecting improved tracking precision; the Barrier Function-Based SMC consistently yields the smallest RMS errors (0.11 for e_1 and 0.34 for e_2). Furthermore, in terms of control effort, the proposed controllers exert smoother and less aggressive control actions, again with the barrier function-based SMC requiring the lowest overall effort ($u_1 = 2.81$, $u_2 = 9.31$) compared with the higher values in ERLSMC ($u_1 = 3.26$, $u_2 = 9.38$). These results substantiate the efficiency and robustness of the proposed control strategies, demonstrating that among all examined designs, the barrier function-based SMC provides the most favorable balance between speed, accuracy, and control smoothness.

5 Conclusion

In this paper, a robust finite-time barrier function-based sliding mode control scheme was proposed to address the trajectory tracking problem of autonomous sailboats subject to environmental disturbances. By introducing a novel fast-reaching law, the proposed method successfully decoupled the trade-off between convergence speed and chattering reduction. Theoretical analysis grounded in Lyapunov stability theory confirmed the finite-time convergence properties of the system. Moreover, comparative simulations demonstrated that the proposed approach reduces the settling time by approximately 39.4% and the RMS error by 38.9% compared to the ERLSMC method. Future research directions will focus on extending this framework to multi-agent sailboat formations and incorporating adaptive neural networks to estimate hydrodynamic coefficients in real-time.

Declarations

Funding

This research received no specific grant from any funding agency in the public, commercial, or not-for-profit sectors.

Conflict of Interest

The authors declare that they have no known competing financial interests or personal relationships that could have appeared to influence the work reported in this paper.

Ethical Approval

This article does not contain any studies with human participants or animals performed by any of the authors.

Author Contributions

Mohammad Reza Jalili: Conceptualization, Methodology, Software, Validation, Formal analysis, Investigation, Writing – Original Draft.

Ahmad Reza Vali: Conceptualization, Methodology, Resources, Writing – Review & Editing, Supervision, Project administration.

Mohammad Ali Alirezapouri: Conceptualization, Methodology, Software, Validation, Formal analysis, Writing – Review & Editing.

Hossein Nourmohammadi: Conceptualization, Methodology, Software, Validation, Formal analysis, Investigation, Writing – Review & Editing.

Data Availability

No datasets were generated or analyzed during the current study. The simulation parameters and model details are fully described in the manuscript, and the MATLAB/Simulink code used for simulations is available from the corresponding author upon reasonable request.

Informed Consent

Not applicable.

Use of AI and AI-Assisted Technologies

During the preparation of this work, the authors used AI-assisted tools (e.g., grammar and style checkers) solely for language refinement and proofreading. After using these tools, the authors reviewed and edited the content as needed and take full responsibility for the final content of the publication.

References

Abrougui H, Dallagi H, Nejim S (2019a) Autopilot design for an autonomous sailboat based on sliding mode control. Autom Control Comput Sci 53(5):393–407. https://doi.org/10.3103/S0146411619050031

Abrougui H, Nejim S, Dallagi H (2019b) Modeling and autopilot design for an autonomous catamaran sailboat based on feedback linearization. In: 2019 International Conference on Advanced Systems and Emergent Technologies (IC_ASET), Hammamet, Tunisia, pp 130-135. http://doi.org/10.1109/ASET. 2019.8871049

Ames AD, Xu X, Grizzle JW, Tabuada P (2016) Control barrier function based quadratic programs for safety critical systems. IEEE Trans Autom Control 62(8):3861–3876. https://doi.org/10.1109/TAC. 2016.2638961

Chen M, Ge SS, How BVE, Choo YS (2013) Robust adaptive position mooring control for marine vessels. IEEE Trans Control Syst Technol 21(2):395–409. https://doi.org/10.1109/TCST. 2012.2183676

Fallaha CJ, Saad M, Kanaan HY, Al-Haddad K (2011) Sliding-mode robot control with exponential reaching law. IEEE Trans Ind Electron 58(2):600–610. https://doi.org/10.1109/TIE.2010.2045995

Huang J, Ye Z, Ni H, Zhang D, Abdulaal M (2024) Finite-time resilient sliding mode control of UMV systems with stochastic actuator failures and DoS attacks. Trans Inst Meas Control 47(2):345–358. https://doi.org/10.1177/01423312241242840

Jalili MR, Vali AR, Alirezapouri MA, Nourmohammadi H (2024) Motion control of an unmanned sailing boat subject to surface disturbances based on an integrated optimal feedback linearization algorithm. Hydrophysics 10(1):67–82. https://doi.org/20.1001.1.24767131.1403.10.1.6.8

Jaulin L, Le Bars F (2013) A simple controller for line following of sailboats. In: Robotic Sailing 2013. Springer, Cham, pp 11–22. https://doi.org/10.1007/978-3-642-33084-1_11

Jaulin L, Le Bars F (2014) Sailboat as a windmill. In: Le Bars F, Jaulin L (eds) Robotic Sailing 2013. Springer, Cham, pp 81–92. https://doi.org/10.1007/978-3-319-02276-5_7

Meng X, Zhang G, Han B (2024) Fault-tolerant control of underactuated MSVs based on neural finite-time disturbance observer: an event-triggered mechanism. J Franklin Inst 361(4):1067–1085. https://doi.org/10.1016/j.jfranklin.2024.01.004

Moulay E, Léchappé V, Bernuau E, Plestan F (2022) Robust fixed-time stability: application to sliding-mode control. IEEE Trans Autom Control 67(2):1061–1066. https://doi.org/10.1109/TAC.2021.3055440

Nourmohammadi H, Sabet M (2025) Auto-calibrated adaptive integrated AHRS/TAM system for orientation estimation of long-range AUVs. Expert Syst Appl 288:128186. https://doi.org/10.1016/j.eswa.2025.128186

Ovalle L, González A, Fridman L, Laghrouche S, Obeid H (2025) Analysis of barrier function based adaptive sliding mode control in the presence of deterministic noise. Automatica 171:111946. https://doi.org/10.1016/j.automatica.2024.111946

Sabet K, Nourmohammadi H (2026) Modified artificial field method based on leader-follower strategy for multi-AUVs formation control and path planning. Ocean Engineering and Marine Energy 12(1):401–414. https://doi.org/10.1007/s40722-025-00436-3

Shao K, Zheng J, Tang R, Li X, Man Z, Liang B (2022) Barrier function based adaptive sliding mode control for uncertain systems with input saturation. IEEE/ASME Trans Mechatron 27(5):4258–4268. https://doi.org/10.1109/TMECH.2022.3153670

Shi Q, Wang R, Li X, Yang J (2024) Barrier Lyapunov function-based adaptive optimized control for full-state and input-constrained dynamic positioning of marine vessels with simulation and model-scale tests. Ocean Eng 301:117534. https://doi.org/10.1016/j.oceaneng.2024.117534

Sun Z, Feng A, Yu J, Zhao W, Huang Y (2025) Development of autonomous sailboat sails and future perspectives: a review. Renew Sustain Energy Rev 207:114918. https://doi.org/10.1016/j.rser.2024.114918

Tipsuwan Y, Sanposh P, Techajaroonjit N (2023) Overview and control strategies of autonomous sailboats – a survey. Ocean Eng 281:114879. https://doi.org/10.1016/j.oceaneng.2023.114879

Wang W, Wen T, He X, Xu G (2023) Path following with prescribed performance for under-actuated autonomous underwater vehicles subject to unknown actuator dead-zone. IEEE Trans Intell Transp Syst 24(6):6257–6267. https://doi.org/10.1109/TITS.2023.3267534

Yan Y, Zhao X, Yu S, Wang C (2021) Barrier function-based adaptive neural network sliding mode control of autonomous surface vehicles. Ocean Eng 238:109684. https://doi.org/10.1016/j.oceaneng.2021.109684

Zhang Z, Guo N, Zhu S, Jiao F, Gong D, Song X (2025) A model-free and finite-time active disturbance rejection control method with parameter optimization. Expert Syst Appl 278:127370. https://doi.org/10.1016/j.eswa.2025.127370

Zhu G, Ma Y, Hu S (2020) Single-parameter-learning-based finite-time tracking control of underactuated MSVs under input saturation. Control Eng Pract 105:104652. https://doi.org/10.1016/j.conengprac.2020.104652